

基于多通道 FP-FBG 的波长可切换单纵模掺铥光纤激光器

王伟利, 延凤平*, 张鲁娜

北京交通大学光波技术研究所全光网络与现代通信网教育部重点实验室, 北京 100044

摘要 对 2 μm 波段的法布里-珀罗光纤光栅进行了仿真分析和实验制作;设计并搭建了一种基于多通道法布里-珀罗光纤光栅滤波器的三波长间可切换的单纵模复合腔掺铥光纤激光器。激光谐振腔内使用两个光耦合器组成的 8 字环无源子腔来扩大纵模间隔;使用自制法布里-珀罗光纤光栅滤波器进行波长选择,并利用偏振控制器调节腔内损耗以抑制光纤激光的强模式竞争;通过应力调节架调节均匀光纤光栅,实现了三个波长间切换的单纵模激光运转。实验结果表明:在室温时,该掺铥光纤激光器可获得输出波长分别为 1941.48 nm、1941.57 nm 和 1941.65 nm,对应光信噪比分别为 61 dB、61 dB 和 60 dB 的稳定的可切换单纵模激光输出。分别对三个波长的激光进行连续 50 min 的稳定性测量,得到激光输出功率的波动分别小于 0.39 dB、0.61 dB 和 0.55 dB,波长波动小于光谱仪的最小分辨率 0.05 nm,说明该激光器具有良好的稳定性。

关键词 激光光学;掺铥光纤激光器;单纵模;复合腔;光纤光栅;法布里-珀罗光纤光栅滤波器

中图分类号 TN248.1

文献标志码 A

doi: 10.3788/CJL202148.2101001

1 引言

掺铥光纤激光器(TDFL)的工作波长在 2.0 μm 波段,是人眼安全的工作波段^[1],且其中存在高透过率的大气窗口和多种气体分子以及 OH^- 离子的强吸收峰。因此,TDFL 在空间光通信、气体传感和检测、激光手术刀等领域具有广阔的应用前景^[2-4]。其中,窄线宽光纤激光器在长距离光纤传感^[1]、相干光通信^[5]、光载无线电^[6]、高精度光谱表征、激光雷达^[7]、光纤遥感等领域具有重要应用^[8]。而波长可切换的光纤激光器以其输出波长的灵活性,可以应用在光通信的波分复用(WDM)系统和多参量传感系统中^[9-10]。可见,波长可切换的窄线宽 TDFL 具有巨大的潜在应用价值。

目前,国内外获得波长可切换光纤激光器的主要方法有弯曲依赖损耗方法^[11]、声波技术^[12]、基于级联光纤布拉格光栅(FBG)的方法^[13]以及利用光子晶体光纤的方法^[14-15]等。其中,FBG 被视为窄带

滤波器^[16],通过 FBG 反射的光波损耗小,可忽略。FBG 以光纤为基质,具有体积小、成本低、稳定性高、与光纤兼容等优点,这使其成为全光纤激光器波长选择元件的首选^[17]。通过外力改变光纤光栅的长度,使光栅的周期发生改变,进而使其工作波长发生偏移,该调节方法操作简单且高效,可用于调节光纤激光器的输出激光波长^[18-19]。窄线宽激光输出的前提是激光器的单纵模(SLM)运转。目前,实现光纤激光器单纵模输出的方法有饱和吸收体法^[20-24]、复合腔法^[25-26]、滤波器法^[27-28]、短腔选模法^[29-31]等。在光纤激光器腔型设计中,常用的超短腔结构激光器有分布反馈式激光器和分布布拉格反射激光器^[32-34],然而这些激光器的腔长较短,难以获得较高的输出功率,不易加入其他器件用于进一步提升性能;再者使用可饱和吸收体作为窄带滤波器^[35],在腔内使用一段未泵浦的增益光纤作为可饱和吸收体,这样可实现激光器单纵模运转,但同时会在腔内引入较大损耗,导致激光器的输出功率较低。不同

收稿日期: 2021-02-25; 修回日期: 2021-03-23; 录用日期: 2021-04-12

基金项目: 国家自然科学基金(61827818, 61620106014, 61775128)

通信作者: *fpyan@bjtu.edu.cn

类型的复合腔结构是现在的研究热点之一^[36-38]。在主腔中加入子环形腔,可有效地增大纵模间隔,而且环形腔还具有结构简单、可调谐性良好、泵浦效率较高等优点。本课题组已在窄线宽 TDFL 方面做了相关研究^[23,39]。2019 年,王雪等^[40]提出了基于复合腔法和 FBG 设计的单纵模窄线宽 TDFL,该器件由 3 个互相连接的光耦合器(coupler)组成子腔,抑制密集的多纵模和跳模,实现了中心波长为 1940.6 nm、光信噪比(OSNR)为 60 dB 的稳定激光输出。

本文提出并通过实验验证了一种基于多通道 FP-FBG 的三个波长间可切换的 SLM TDFL。分析了该单纵模光纤激光器的实现原理,其基于由主环腔和 8 字次级腔(8 字腔)组成的多环配置、通过使用自制的窄线宽 FP-FBG 滤波器实现 SLM 运转;通过改变 FBG 反射中心波长实现波长可切换功能,结合激光器腔内偏振态调控,使波长可切换 TDFL 能够以高稳定性和超高 OSNR 运行。此外,在室温条件下分析了该 TDFL 分别在三个波长模式下输出的 SLM 特性,并对激光的稳定性等输出特性进行了观察和测量。

2 仿真和实验理论

2.1 光栅的仿真和制作

通过使用两个具有相同中心波长的 FBG 构成 FP-FBG,可以完成良好的模式选择,FP-FBG 的透射率为^[41]

$$T_{\text{FP-FBG}} = \frac{1}{1 + F \sin^2(\beta h - \varphi_p)}, \quad (1)$$

式中: $F = 4R/(1-R)^2$,其中 R 是均匀 FBG 的反射率; h 为两个光纤光栅之间的距离; φ_p 为光纤光栅反射率相移因子; β 是传输常数。由光纤光栅的耦合模理论可得^[42]

$$R = \frac{\sinh^2(\sqrt{\kappa^2 - \hat{\sigma}^2} L_g)}{\cosh^2(\sqrt{\kappa^2 - \hat{\sigma}^2} L_g) - \hat{\sigma}^2/\kappa^2}, \quad (2)$$

式中: L_g 为 FBG 的长度; $\kappa = \pi v \delta \bar{n}_{\text{eff}}/\lambda$ (其中 v 为折射率调制的条纹可见度, λ 为波长, $\delta \bar{n}_{\text{eff}}$ 为常数,对应光纤光栅一个周期内平均有效折射率的变化); $\hat{\sigma} = \delta + \sigma - 0.5 d\Phi/dz$ [其中 $\delta = \beta - \pi/\Lambda = 2\pi n_{\text{eff}}(1/\lambda - 1/\lambda_D)$, λ_D 为周期是 Λ 的 FBG 的反射中心波长, n_{eff} 为有效折射率]。因为均匀 FBG 沿 z 方向均匀分布,因而 $d\Phi/dz = 0$ 。取两个相同 FBG 的长度 L_g 为 18 mm,FP-FBG 腔长 h 为 6.4 mm,折射率调制的条纹可见度 v 为 1,平均有效折射率 $\delta \bar{n}_{\text{eff}}$ 为

8×10^{-5} ,纤芯的有效折射率 n_{eff} 为 1.45,FBG 的中心波长 λ_D 为 1940 nm,仿真得到 FP-FBG 的透射谱如图 1 所示。由图 1 可知,FP-FBG 滤波器的透射谱产生了三个透射通道,左侧透射通道的中心波长为 1939.91 nm,3 dB 带宽约为 0.015 nm,中间透射通道的中心波长为 1940 nm,3 dB 带宽约为 2×10^{-3} nm,右侧透射通道的中心波长为 1940.9 nm,3 dB 带宽约为 0.015 nm,该 FP-FBG 滤波器的阻带内产生三个几乎无损耗的透射峰,将 FBG 当作一个带阻滤波器,在二者的共同作用下可对光谱进行波长选择与窄带滤波。

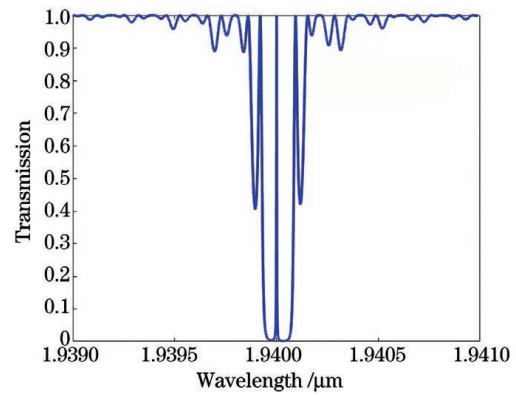


图 1 FP-FBG 的透射谱

Fig. 1 Transmission spectrum of FP-FBG

分析 FP-FBG 的透射谱随腔长 h 的变化,取 FP-FBG 的腔长 h 分别为 2, 6, 10, 16 mm,FBG 的长度 L_g 为 18 mm,折射率调制的条纹可见度 v 为 1,平均有效折射率 $\delta \bar{n}_{\text{eff}}$ 为 8×10^{-5} ,纤芯的有效折射率 n_{eff} 为 1.45,FBG 的中心波长 λ_D 为 1940 nm,仿真得到的 FP-FBG 透射谱如图 2 所示。当腔长比较小时,FP-FBG 腔长比较短,两个相邻峰的间隔比较大,在光栅的透射谱范围内只出现 1 个峰;腔长增大时,两个相邻峰的间隔减小,其透射谱峰的数目也增加,当腔长增大到一定值时,腔内三个模式运转,即实现三波长滤波。

分析 FP-FBG 的透射谱随 FBG 长度 L_g 的变化,取 FBG 的长度 L_g 分别为 24, 18, 8, 4 mm,FP-FBG 腔长 h 为 6.4 mm,折射率调制的条纹可见度 v 为 1,平均有效折射率 $\delta \bar{n}_{\text{eff}}$ 为 8×10^{-5} ,纤芯的有效折射率 n_{eff} 为 1.45,FBG 的中心波长 λ_D 为 1940 nm,仿真得到的 FP-FBG 透射谱如图 3 所示。当 FBG 的长度 L_g 较小时,反射率较低,FP-FBG 腔的带宽较宽;FBG 的长度 L_g 的增大时,FP-FBG 腔的带宽变窄,透射峰的数目增加,其透射谱的旁瓣效应变得明显,FBG 的长度 L_g 增大到一定值时,腔内

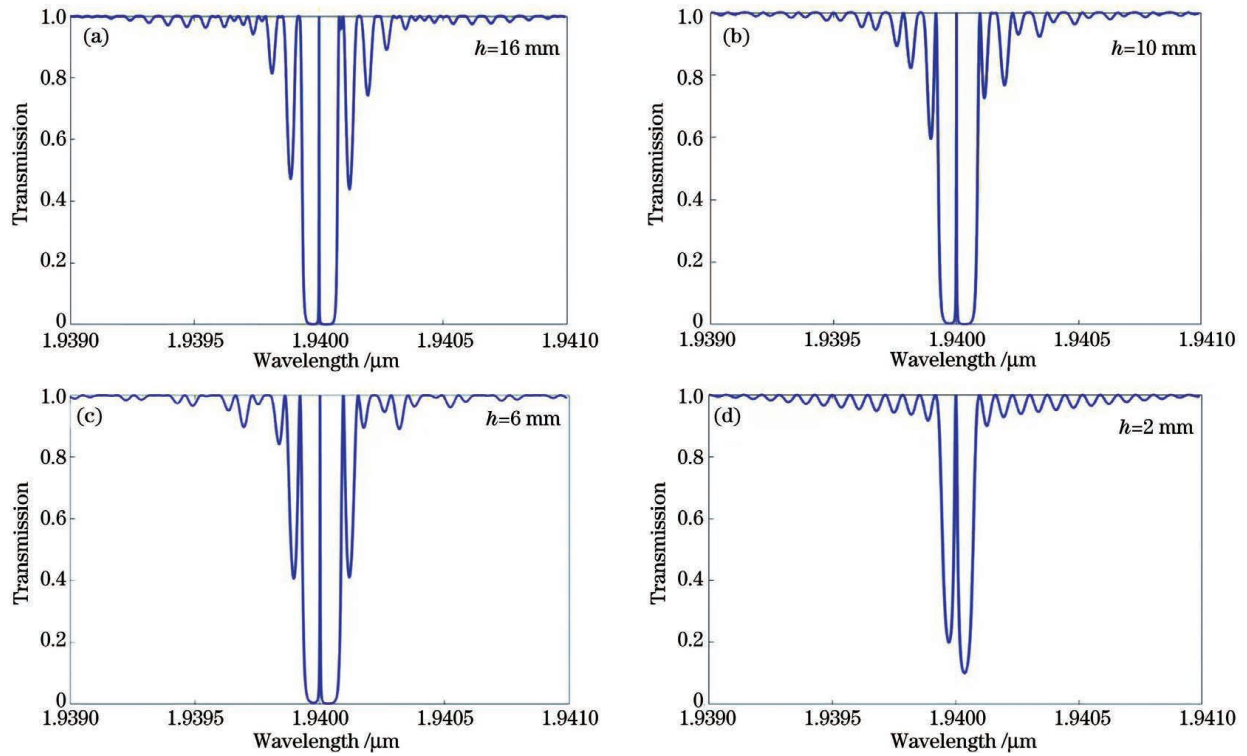


图 2 h 变化时 FBG F-P 的透射谱。(a)16 mm;(b)10 mm;(c)6 mm;(d)2 mm

Fig. 2 Transmission spectra of FBG F-P when h changes. (a) 16 mm; (b) 10 mm; (c) 6 mm; (d) 2 mm

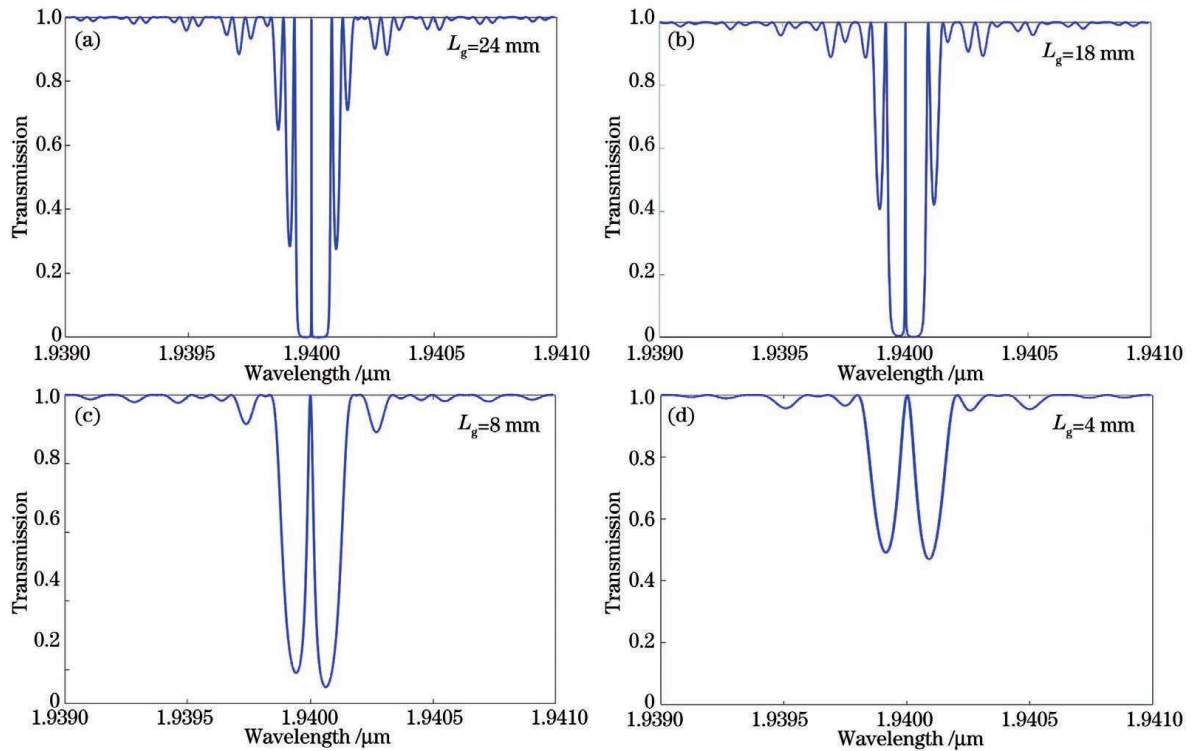


图 3 L_g 变化时 FBG F-P 的透射谱。(a)24 mm;(b)18 mm;(c)8 mm;(d)4 mm

Fig. 3 Transmission spectra of FBG F-P when L_g changes. (a) 24 mm; (b) 18 mm; (c) 8 mm; (d) 4 mm

有三个模式运转,即实现三波长滤波。

分析 FP-FBG 的透射谱随平均有效折射率 $\delta \bar{n}_{\text{eff}}$ 的变化。取平均有效折射率 $\delta \bar{n}_{\text{eff}}$ 分别为 6×10^{-5} ,

7×10^{-5} , 8×10^{-5} , 9×10^{-5} , FBG 的长度 L_g 为 18 mm, FP-FBG 腔长 h 为 6.4 mm, 折射率调制的条纹可见度 v 为 1, 纤芯的有效折射率 n_{eff} 为 1.45,

FBG 的中心波长 λ_D 为 1940 nm, 仿真得到的 FP-FBG 透射谱如图 4 所示。 δn_{eff} 增大时, FP-FBG 光谱透射峰深度增加, 透射峰宽度逐渐减小, 阻带宽度增加。

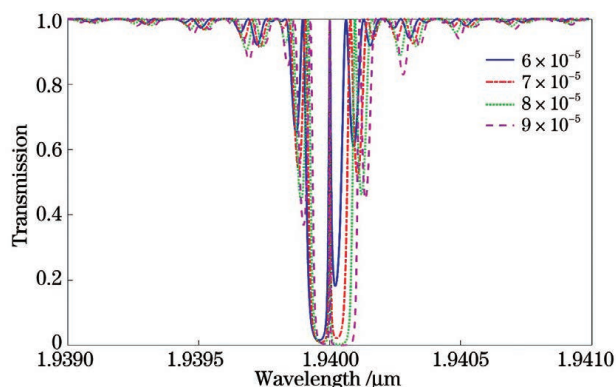


图 4 δn_{eff} 变化时 FBG F-P 的透射谱

Fig. 4 Transmission spectra of FBG F-P when δn_{eff} changes

在激光器实验中, 除 FP-FBG 外还须使用一个窄带 FBG 进行波长选择, 实验中的 FBG 和 FP-FBG 均采用相位掩模法^[43]制作, 实验时根据掩模版实际长度(25 mm)制作所用的光栅, 掩模版周期为 1347.3 nm, 光斑的直径为 5 mm, 有部分实验数据和仿真数据不一致。FP-FBG 中两个栅区的长度均为 10 mm, 光栅参数完全一致, 其间隔为 4 mm, 总长度为 24 mm。FBG 的光栅长度为 20 mm。利用掺铒光纤(TDF)的放大自发辐射(ASE)作为光源, 用光谱分析仪(OSA, YOKOGAWA AQ6375, 分辨率为 0.05 nm)对 FBG 的反射谱以及 FP-FBG 的透射谱进行测量, 得到的光谱分别如图 5 所示。其中实线为 FP-FBG 的透射谱, 它有三个窄带滤波通道(C-1、C-2 和 C-3), 其透射波长分别为 1941.48 nm (λ_1)、1941.57 nm (λ_2) 和 1941.65 nm (λ_3), 对应的 3 dB 带宽分别为 0.06 nm、0.054 nm 和 0.066 nm。图 5 中其余三条曲线表示通过应力调节架拉伸后的

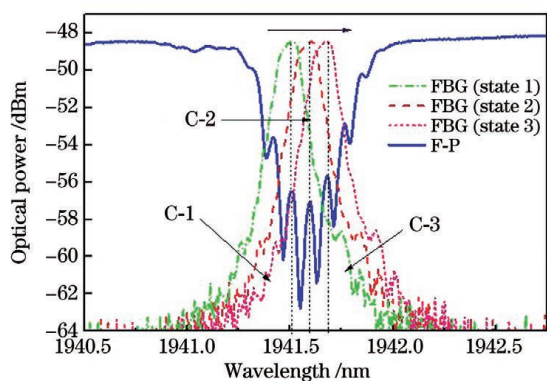


图 5 FBG 的反射光谱和 FP-FBG 的透射光谱

Fig. 5 FBG reflection spectrum and transmission spectra of FP-FBGs

FBG 反射谱。FBG 的中心波长向长波长方向移动, 该 FBG 的 3 dB 带宽为 0.11 nm, 光栅反射率约为 97%。通过调节 FBG 的中心波长分别与 FP-FBG 的三个透射通道中心波长一致, 使该滤波通道中心波长处的光反射率最高, 因此, 可选择与 FP-FBG 滤波器透射通道中心波长一致的单纵模激光输出, 同时, FP-FBG 滤波器的三个滤波通道带宽很窄, 起到减小输出单纵模激光线宽的作用, 从而起到选频的作用。

2.2 激光器实验结构

所提出的波长可切换 SLM TDFL 结构如图 6 所示。激光二极管(LD)作为泵浦源通过光纤合束器(FC)对一段长为 2 m 的掺铒光纤(TDF)进行泵浦, TDF 的纤芯和包层直径分别为 10 μm 和 130 μm 。环形器(circulator)用来确保环形腔内的光路单向运行。环形器的 2 端口处连接 FBG, FBG 放置在应力调节架上, 通过结合腔内一个具有窄带滤波功能的三通道 FP-FBG 滤波器, 可以抑制大部分的激光纵模。通过应力调节架改变 FBG 的反射波长, 使其分别与 FP-FBG 滤波器三个通道重叠, 从而实现三个波长可切换的稳定激光输出。PC 用来调节腔内信号的偏振态, 平衡腔内增益和损耗, 使输出激光达到最大 OSNR 并实现稳定输出。两个 50 : 50 的 coupler 构成 8 字子腔, 在主腔中插入 8 字子腔, 可以有效地增大纵模间隔, 减少多纵模和跳模^[20], 该方法具有很好的 SLM 选择能力。通过合理地调整各个谐振腔长度, 实现了光纤激光器的 SLM 输出。激光器的输出功率和谐振腔输出的光谱线宽受光纤耦合器的耦合比影响, 当输出功率满足要求时, 提高光纤耦合器的耦合比或使用耦合比更大的一端作为

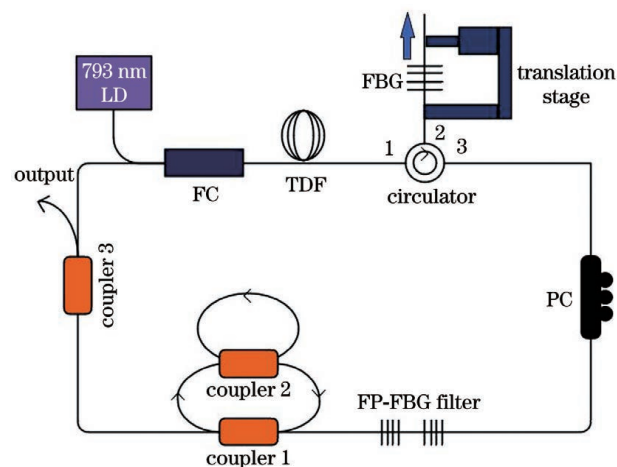


图 6 波长可切换 SLM TDFL 的结构图

Fig. 6 Structural diagram of wavelength-switchable SLM TDFL

谐振腔的输入端均可起到抑制多纵模和跳模的作用,从而实现更窄的光谱线宽输出^[44]。因此,激光器使用 90 : 10 的耦合器输出激光,其中,耦合器的 10% 端口为输出端,90% 的一端连接主腔。激光器主腔的腔长约为 12 m,对应的纵模间隔为 17.2 MHz。

激光器选取 SLM 原理图如图 7 所示。图 7(a) 表示增益介质的增益带宽,图 7(b) 中环形腔内纵模间隔为 17.2 MHz,图 7(c) 表示 FBG 的增益带宽为 0.11 nm,此时增益带宽内仍具有多个纵模,图 7(d) 表示 FP-FBG 的滤波带宽。两个 50 : 50 的光耦合器构成 8 字子腔,其中,2 个子环形腔的腔长分别为 0.25 m 和 0.35 m,对应的自由光谱范围(FSR)分别为 820 MHz 和 600 MHz,由游标效应^[45]可以计算出 8 字子腔的 FSR 为 24.6 GHz,经单位转换后得到该子腔在 1940 nm 处对应的纵模间隔约为

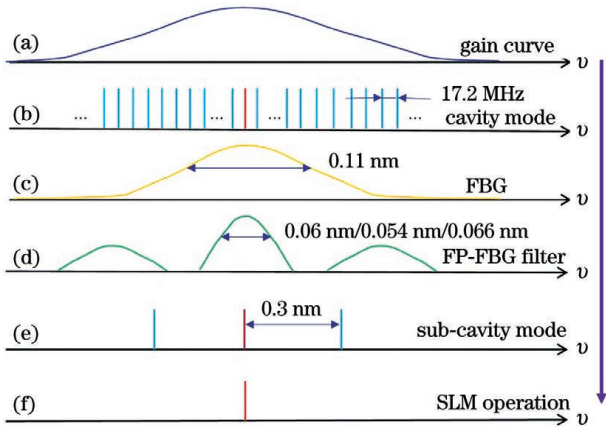


图 7 光纤激光器选取单纵模的原理示意图

Fig. 7 Schematic of single longitudinal mode selection of fiber laser

0.3 nm,如图 7(e)所示,该间隔大于 FP-FBG 三个透射谱的 3 dB 带宽,可以确保每个通道的 SLM 激光。腔内纵模间隔与谐振腔长度和类型有关,因此,通过子腔扩大纵模间隔,并结合窄带滤波器滤除多余纵模,最终只能有一个纵模在腔内振荡,其他纵模均被抑制,如图 7(f)所示。利用 PC 平衡腔内信号的增益与损耗,结合窄带滤波器和复合腔,理论上保证了该 TDFL 的 SLM 稳定运转。实现波长切换的原理为:使用应力调节架对 FBG 施加轴向应力,通过改变光栅周期,即可调节窄带 FBG 的反射波长,如图 5 中箭头所示。随着应力的增大,FBG 反射波长向长波长方向漂移。当其反射波长与 FP-FBG 的不同通道重叠,该波长处的光在腔内振荡并输出。通过调节应力调节架改变 FBG 上的应力,可以实现不同激光波长之间的切换。

3 实验结果与分析

在室温(24 °C)条件下,将该激光器搭建在光学防震平台上的一块金属散热板上,实验测得所设计的 TDFL 的阈值功率为 1.68 W,当泵浦源功率为 2.34 W 时,调整应力调节架,将 FBG 反射谱包络向长波长方向移动,使反射峰分别与 FP-FBG 滤波器的三个通道的中心波长一致,通过调节 PC,可分别得到三个波长激光的稳定输出。将 TDFL 的输出端连接到分辨率为 0.05 nm 的 OSA 进行测量,得到稳定的激光输出光谱,如图 8 所示,激光波长分别为 1941.48 nm(λ_1)、1941.57 nm(λ_2)和 1941.65 nm(λ_3),与 FP-FBG 滤波器三个通道的中心波长一致。激光输出的 OSNR 分别为 61 dB、61 dB 和 60 dB。

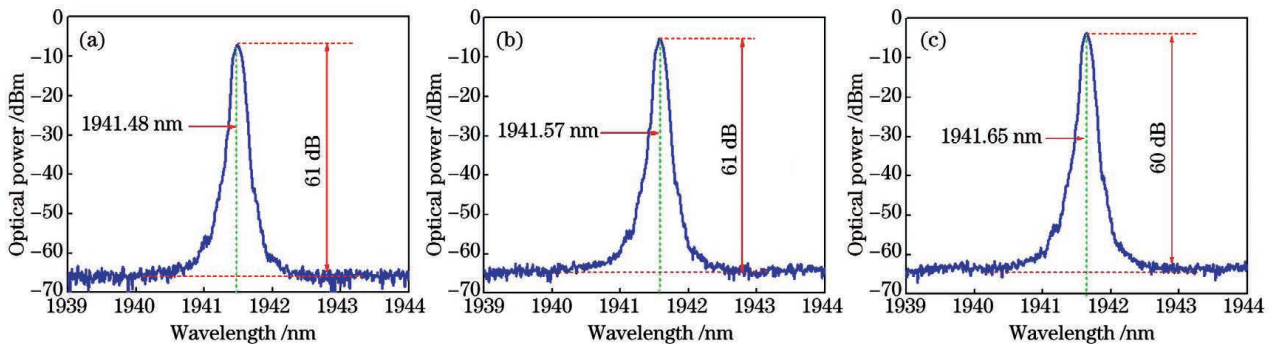


图 8 三个波长的激光输出光谱。(a)1941.48 nm;(b)1941.57 nm;(c)1941.65 nm

Fig. 8 Laser output spectra of three center wavelengths. (a) 1941.48 nm; (b) 1941.57 nm; (c) 1941.65 nm

为了观察该激光器的稳定性,分别对三个波长的激光光谱进行 10 次连续扫描(记为 B~K),扫描时间间隔为 5 min,光谱如图 9 所示。对测量数据进行分析,可以得到 50 min 内激光输出功率

和波长的波动情况,结果如图 10 所示。 λ_1 、 λ_2 和 λ_3 处激光的中心波长波动均小于 0.01 nm,且三个波长的激光功率波动分别小于 0.39 dB、0.61 dB 和 0.55 dB。由此可知,该激光器在室温环境下具

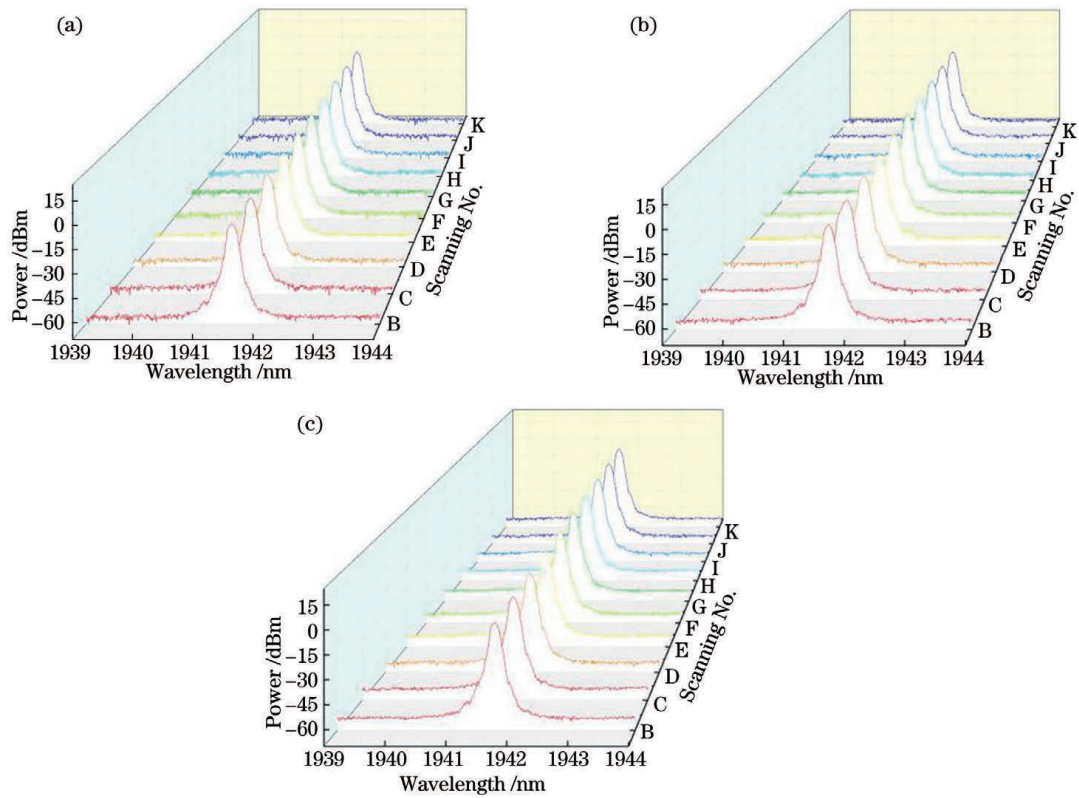


图 9 输出激光间隔 5 min 的 10 次连续扫描光谱。(a)1941.48 nm;(b)1941.57 nm;(c)1941.65 nm

Fig. 9 Output spectra of 10 consecutive scans with 5 min interval. (a) 1941.48 nm; (b) 1941.57 nm; (c) 1941.65 nm

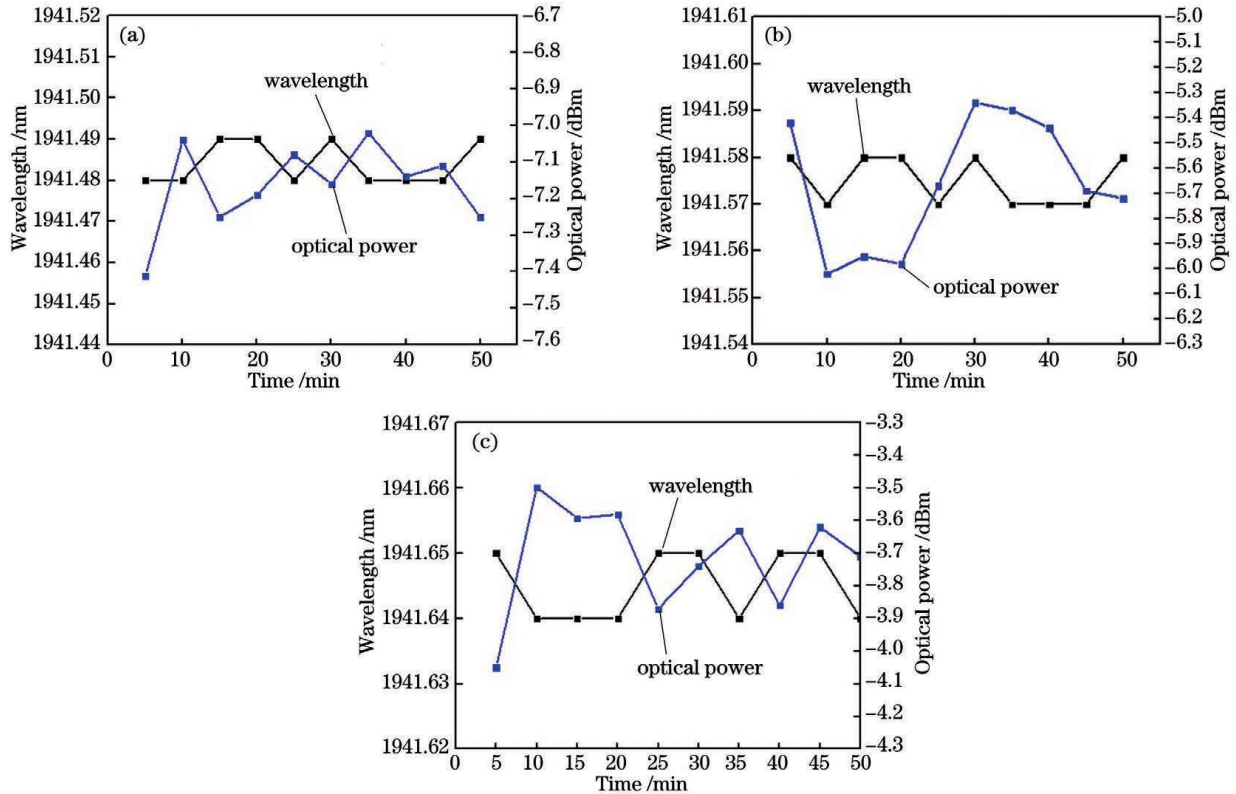


图 10 TDFL 的输出功率和中心波长随时间的变化。(a)1941.48 nm;(b)1941.57 nm;(c)1941.65 nm

Fig. 10 Output power and center wavelength of TDFL change with time. (a) 1941.48 nm; (b) 1941.57 nm; (c) 1941.65 nm

有良好的稳定性,可以实现 50 min 内的稳定工作。中心波长和峰值功率的波动主要是环境中声音振动、LD 输入功率波动和 OSA 分辨率限制等因素引起的无规则变动。

为了观察输出激光的单纵模特性,使用频谱分析仪(ESA)对输出激光的频谱进行了测量。将激光器输出端连接到一个 1 GHz 的光电探测器(PD)上,把光信号转换为电信号,然后由 ESA 检测该电信号,同时用分光光路将激光器输出端连接到

OSA,用以实现激光光谱和频谱的同时测量。图 11 为所测激光的频谱图,ESA 的扫描范围为 500 MHz,分辨率为 10 kHz,测量过程中泵浦功率固定为 2.34 W。如图 11(a)所示,未调节 PC 时该扫描范围内出现多个拍频信号,表明此时激光输出并非为稳定的 SLM 状态。调节 PC 后,三个波长的激光频谱图分别如图 11(b)~(d)所示,可以看出测量范围内并未出现拍频信号,这表明该 TDFL 处于稳定的 SLM 状态。

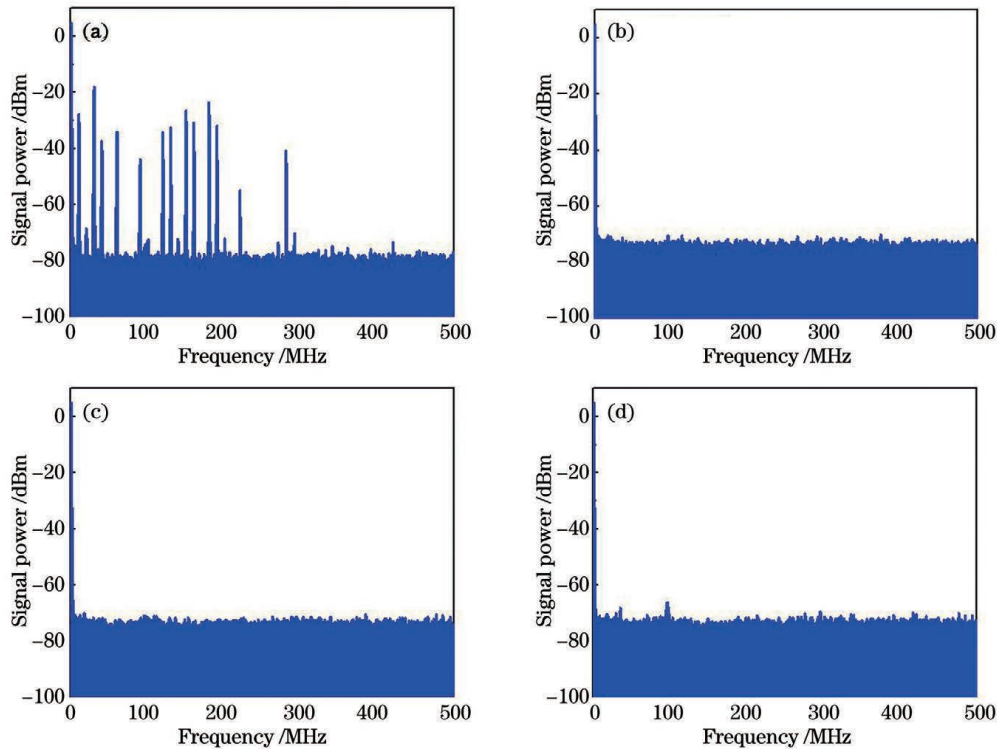


图 11 输出激光频谱图。(a)未调节 PC;(b)1941.48 nm;(c)1941.57 nm;(d)1941.65 nm

Fig. 11 RF spectra of output laser. (a) Unregulated PC; (b) 1941.48 nm; (c) 1941.57 nm; (d) 1941.65 nm

TDFL 在中心波长 λ_1 、 λ_2 和 λ_3 处的输出功率和泵浦功率之间的关系如图 12 所示。激光器阈值功率约为 1.68 W,当泵浦功率为 2.34 W 时,三个波长的输出功率分别为 0.93 mW、1.08 mW 和

1.24 mW,曲线呈良好的线性。由于腔内不同类型光纤熔接点处存在模场失配,激光器的光光转换效率较低。由图可以看出,激光器没有达到饱和,输出功率可随着泵浦功率的增加而继续增加,但考虑到

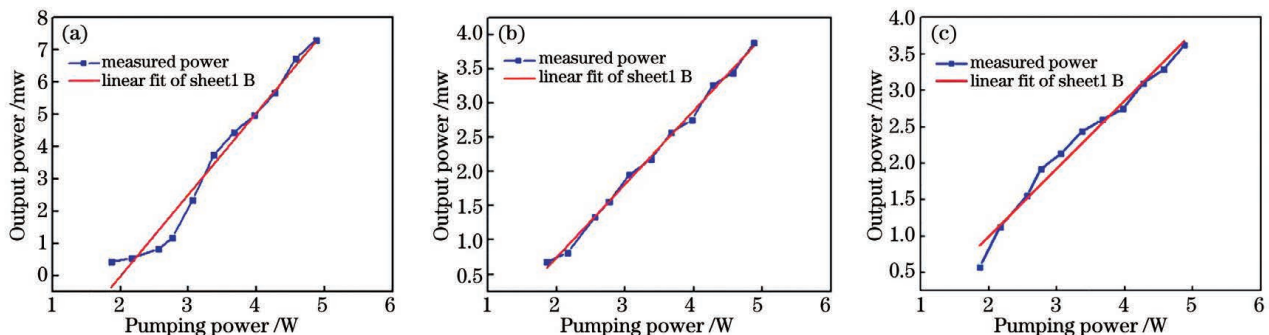


图 12 TDFL 输出功率随泵浦功率的变化。(a)1941.48 nm;(b)1941.57 nm;(c)1941.65 nm

Fig. 12 Output power of TDFL varying with pump power. (a) 1941.48 nm; (b) 1941.57 nm; (c) 1941.65 nm

TDF 熔接点和腔内器件的承受能力,最大泵浦功率只设定为 5 W。

4 结 论

实验验证了一种基于多通道 FP-FBG 滤波器的波长可切换单纵模 TDFL。将自制的窄带 FBG 和 FP-FBG 滤波器与 8 字行子腔相结合,二者的共同作用可实现 TDFL 波长可切换的单纵模激光输出。同时,用 PC 抑制强模式竞争,抑制掉较弱的波长成分。通过调整应力调节架,使输出激光在三个波长之间切换,在室温条件下获得中心波长分别为 1941.48 nm、1941.57 nm 和 1941.65 nm 的激光输出,其 OSNR 分别为 61 dB、61 dB 和 60 dB。在 50 min 的测量时间内,每个激光波长的波动均小于 0.01 nm,小于 OSA 的最小分辨率(0.05 nm),激光输出功率的波动分别小于 0.39 dB、0.61 dB 和 0.55 dB。通过采用良好的隔振和温度补偿方法可进一步提升该 TDFL 的性能。所提出的 3 个波长可切换的掺铥光纤激光器具有稳定的单纵模特性,可以应用于 2.0 μm 波段的光通信和光纤传感等领域。

参 考 文 献

- [1] Zhang W, Zhang J Y, Yu T, et al. Research progress of 2 μm high-power continuous thulium-doped fiber laser [C] // 2016 Infrared and Remote Sensing Technology and Application Seminar and Interdisciplinary Forum Proceedings, December 6, 2016, Changzhou, Jiangsu, China. Shanghai: Shanghai Society of Infrared and Remote Sensing, 2016: 244-249.
张伟, 张嘉阳, 余婷, 等. 2 μm 高功率连续掺铥光纤激光器研究进展[C] // 2016 年红外、遥感技术与应用研讨会暨交叉学科论坛论文集, 江苏常州. 上海: 上海红外与遥感协会, 2016: 244-249.
- [2] McAleavey F J, O'Gorman J, Donegan J F, et al. Narrow linewidth, tunable Tm^{3+} -doped fluoride fiber laser for optical-based hydrocarbon gas sensing [J]. IEEE Journal of Selected Topics in Quantum Electronics, 1997, 3(4): 1103-1111.
- [3] Shi W, Fang Q, Zhu X S, et al. Fiber lasers and their applications [J]. Applied Optics, 2014, 53(28): 6554-6568.
- [4] McAleavey F J, O'Gorman J, Donegan J F, et al. Extremely high sensitivity gas detection at 2.3 μm using a grazing incidence Tm^{3+} fibre laser cavity [J]. Sensors and Actuators A: Physical, 2001, 87(3): 107-112.
- [5] Li M N, Tan L Y, Yang Q B, et al. Effect of partially coherent laser source on the performance of fiber-coupling DPSK receiver for optical communication [J]. Optics Communications, 2015, 350: 135-143.
- [6] Chen D, Fu J. Microwave photonic filter's application on the microwave signal generation based on an active mode-locked fiber laser [J]. Laser Physics, 2008, 18(11): 1353-1356.
- [7] Swann W C, Newbury N R. Frequency-resolved coherent LIDAR using a femtosecond fiber laser [J]. Optics Letters, 2006, 31(6): 826-828.
- [8] Gordienko V M, Koryabin A V, Kravtsov N V, et al. Wind Doppler lidar with 1.5 μm fiber laser [J]. Laser Physics Letters, 2008, 5(5): 390-393.
- [9] Xu P. Research on ultra-narrow linewidth multi-wavelength fiber laser [D]. Changsha: National University of Defense Technology, 2008.
徐攀. 超窄线宽多波长光纤激光器研究 [D]. 长沙: 国防科学技术大学, 2008.
- [10] Han Y G, Tran T V, Kim S H, et al. Multiwavelength Raman-fiber-laser-based long-distance remote sensor for simultaneous measurement of strain and temperature [J]. Optics Letters, 2005, 30(11): 1282-1284.
- [11] Chen S P, Ding L, Wang S M, et al. Switchable dual-wavelength erbium-doped fiber ring laser using bending dependent loss to switch the operating wavelength [J]. Laser Physics Letters, 2006, 3(12): 584-587.
- [12] Delgado-Pinar M, Mora J, Diez A, et al. Wavelength-switchable fiber laser using acoustic waves [J]. IEEE Photonics Technology Letters, 2005, 17(3): 552-554.
- [13] Mao Q, Feng S, Liu W, et al. Bistability-mapping for L-band dual-wavelength erbium-doped fiber laser by using fiber loop mirror with polarization controller [J]. IEEE Photonics Technology Letters, 2006, 18(18): 1973-1975.
- [14] Chen D, Shen L. Switchable and tunable Erbium-doped fiber ring laser incorporating a birefringent and highly nonlinear photonic crystal fiber [J]. Laser Physics Letters, 2007, 4(5): 368-370.
- [15] Liu Z Y, Liu Y G, Du J B, et al. Channel-spacing and wavelength switchable multi-wavelength erbium-doped fiber laser using sampled Hi-Bi fiber grating and photonic crystal fiber loop mirror [J]. Laser Physics Letters, 2008, 5(2): 122-125.
- [16] Rota-Rodrigo S, Rodríguez-Cobo L, Quintela M Á, et al. Dual-wavelength single-longitudinal mode fiber

- laser using phase-shift Bragg gratings [J]. IEEE Journal of Selected Topics in Quantum Electronics, 2014, 20(5): 161-165.
- [17] Mao L M, Tao C Y, Gu Z D, et al. Dynamic strain sensing system based on fiber ring laser [J]. Acta Optica Sinica, 2019, 39(10): 1006006.
毛黎明, 陶传义, 顾子迪, 等. 基于光纤环形激光器的动态应变传感系统 [J]. 光学学报, 2019, 39(10): 1006006.
- [18] Zhang L N, Yan F P, Feng T, et al. Wavelength-tunable thulium-doped fiber laser with sampled fiber Bragg gratings [J]. Optics & Laser Technology, 2019, 120: 105707.
- [19] Liu S, Yan F P, Peng W J, et al. Tunable dual-wavelength thulium-doped fiber laser by employing a HB-FBG [J]. IEEE Photonics Technology Letters, 2014, 26(18): 1809-1812.
- [20] Cheng Y, Kringlebotn J T, Loh W H, et al. Stable single-frequency traveling-wave fiber loop laser with integral saturable-absorber-based tracking narrow-band filter [J]. Optics Letters, 1995, 20(8): 875-877.
- [21] Meng Z, Stewart G, Whitenett G. Stable single-mode operation of a narrow-linewidth, linearly polarized, erbium-fiber ring laser using a saturable absorber [J]. Journal of Lightwave Technology, 2006, 24(5): 2179-2183.
- [22] Liu J, Yao J P, Yao J, et al. Single-longitudinal-mode multi-wavelength fiber ring laser [J]. IEEE Photonics Technology Letters, 2004, 16(4): 1020-1022.
- [23] Bai Y, Yan F P, Feng T, et al. Ultra-narrow-linewidth fiber laser in $2\ \mu\text{m}$ band using saturable absorber based on PM-TDF [J]. Chinese Journal of Lasers, 2019, 46(1): 0101003.
白燕, 延凤平, 冯亭, 等. 基于保偏掺铥光纤饱和吸收体的 $2\ \mu\text{m}$ 波段超窄线宽光纤激光器 [J]. 中国激光, 2019, 46(1): 0101003.
- [24] Yang J, Qu R H, Sun G Y, et al. A novel single longitudinal mode fiber laser [J]. Chinese Journal of Lasers, 2005, 32(4): 441-444.
杨敬, 瞿荣辉, 孙国勇, 等. 一种新型结构的单纵模光纤激光器 [J]. 中国激光, 2005, 32(4): 441-444.
- [25] Yeh C H, Huang T T, Chien H C, et al. Tunable S-band erbium-doped triple-ring laser with single-longitudinal-mode operation [J]. Optics Express, 2007, 15(2): 382-386.
- [26] Lee C C, Chen Y K, Liaw S K, et al. Single-longitudinal-mode fiber laser using passive multiple-ring-cavity technique [J]. Proceedings of SPIE, 1998, 3420: 253-257.
- [27] Hui Y L, Li Q, Zhang X, et al. Single frequency mode laser controlled by volume Bragg gratings [J]. Chinese Journal of Lasers, 2009, 36(11): 2805-2807.
惠勇凌, 李强, 张翔, 等. 基于体布拉格光栅选模的单纵模激光器 [J]. 中国激光, 2009, 36(11): 2805-2807.
- [28] Chen D, Fu H, Liu W. Single-longitudinal-mode erbium-doped fiber laser based on a fiber Bragg grating Fabry-Perot filter [J]. Laser Physics, 2007, 17(10): 1246-1248.
- [29] Sejka M, Hübner J, Varming P, et al. Distributed feedback Er^{3+} -doped fibre laser [J]. Electronics Letters, 1995, 31(17): 1445-1446.
- [30] Kringlebotn J T, Archambault J L, Reekie L, et al. $\text{Er}^{3+} : \text{Yb}^{3+}$ -codoped fiber distributed-feedback laser [J]. Optics Letters, 1994, 19(24): 2101-2103.
- [31] Qi H F, Song Z Q, Li S J, et al. Apodized distributed feedback fiber laser with asymmetrical outputs for multiplexed sensing applications [J]. Optics Express, 2013, 21(9): 11309-11314.
- [32] Li Y F, Wang C Y, Qi H F, et al. An ultra-narrow linewidth Brillouin fiber laser based on distributed feedback fiber laser [J]. Laser & Optoelectronics Progress, 2020, 57(7): 071401.
李亚方, 王春雨, 祁海峰, 等. 一种基于分布反馈光纤激光器的超窄线宽布里渊光纤激光器 [J]. 激光与光电子学进展, 2020, 57(7): 071401.
- [33] Lu D, Yang Q L, Wang H, et al. Review of semiconductor distributed feedback lasers in the optical communication band [J]. Chinese Journal of Lasers, 2020, 47(7): 0701001.
陆丹, 杨秋露, 王皓, 等. 通信波段半导体分布反馈激光器 [J]. 中国激光, 2020, 47(7): 0701001.
- [34] Qiao C, Su R G, Li X, et al. Design and fabrication of 980 nm distributed Bragg reflection semiconductor laser with high power [J]. Chinese Journal of Lasers, 2019, 46(7): 0701002.
乔闯, 苏瑞巩, 李翔, 等. 980 nm 高功率 DBR 半导体激光器的设计及工艺 [J]. 中国激光, 2019, 46(7): 0701002.
- [35] Kim R K, Chu S, Han Y G. Stable and widely tunable single-longitudinal-mode dual-wavelength erbium-doped fiber laser for optical beat frequency generation [J]. IEEE Photonics Technology Letters, 2012, 24(6): 521-523.
- [36] Feng T, Wang M M, Wang X C, et al. Switchable 0.612-nm-spaced dual-wavelength fiber laser with sub-kHz linewidth, ultra-high OSNR, ultra-low RIN, and orthogonal polarization outputs [J]. Journal of Lightwave Technology, 2019, 37(13): 3173-

- 3182.
- [37] Feng T, Jiang M L, Wei D, et al. Four-wavelength-switchable SLM fiber laser with sub-kHz linewidth using superimposed high-birefringence FBG and dual-coupler ring based compound-cavity filter[J]. *Optics Express*, 2019, 27(25): 36662-36679.
- [38] Zhang L N, Yan F P, Feng T, et al. Six-wavelength-switchable narrow-linewidth thulium-doped fiber laser with polarization-maintaining sampled fiber Bragg grating[J]. *Optics & Laser Technology*, 2021, 136: 106788.
- [39] Sun J H. Research on fiber grating based narrow linewidth thulium-doped fiber laser[D]. Beijing: Beijing Jiaotong University, 2015.
孙景辉. 基于光纤光栅的窄线宽掺铥光纤激光器研究[D]. 北京: 北京交通大学, 2015.
- [40] Wang X, Yan F P, Han W G. Single longitudinal mode narrow linewidth thulium-doped fiber laser with special subring cavity[J]. *Chinese Journal of Lasers*, 2019, 46(9): 0901001.
王雪, 延凤平, 韩文国. 基于特殊子环腔单纵模窄线宽掺铥光纤激光器[J]. *中国激光*, 2019, 46(9): 0901001.
- [41] Guan B O, Yu Y L, Ge C F, et al. Theoretical studies on transmission characteristics of fiber grating Fabry-Perot cavity[J]. *Acta Optica Sinica*, 2000, 20(1): 34-38.
关柏鸣, 余有龙, 葛春风, 等. 光纤光栅法布里-珀罗腔透射特性的理论研究[J]. *光学学报*, 2000, 20(1): 34-38.
- [42] Erdogan T. Fiber grating spectra [J]. *Journal of Lightwave Technology*, 1997, 15(8): 1277-1294.
- [43] Zhang Y S, Yu K, Jiang D S, et al. Fabricating technology of fiber grating with phase masks [J]. *Optical Technology*, 1999, 25(1): 24-27.
张永胜, 郁可, 姜德生, 等. 用相位掩模法制作光纤光栅的技术[J]. *光学技术*, 1999, 25(1): 24-27.
- [44] Dai Z Y. Theoretical and experimental research on the 1.55 μm single-frequency narrow linewidth fiber laser[D]. Chengdu: University of Electronic Science and Technology of China, 2012.
代志勇. 1.55 μm 单频窄线宽光纤激光器理论与实验研究[D]. 成都: 电子科技大学, 2012.
- [45] Lemieux J F, Bellemare A, Latrasse C, et al. Step-tunable (100 GHz) hybrid laser based on Vernier effect between Fabry-Perot cavity and sampled fibre Bragg grating [J]. *Electronics Letters*, 1999, 35(11): 904-906.

Wavelength-Switchable Single-Longitudinal-Mode Thulium-Doped Fibre Laser with Multi-Channel FP-FBG

Wang Weili, Yan Fengping*, Zhang Luna

Key Laboratory of All Optical Network and Advanced Telecommunication Network of Ministry of Education, Institute of Lightwave Technology, Beijing Jiaotong University, Beijing 100044, China

Abstract

Objective The fibre laser working in the eye-safe 2.0- μm band is an important pump source for producing the $\sim 3\text{--}5\ \mu\text{m}$ mid-infrared laser, and the single-longitudinal-mode fibre laser has the characteristics of large gain, good coherence, and stable spectrum. This laser can be applied to laser optical radio, coherent optical communication, optical fibre sensing, optical fibre remote sensing, and other fields having large light source requirements. The wavelength-switchable fibre laser has a flexible output laser wavelength, which has great application value in the wavelength division multiplexing and multi-parameter sensing systems. The single-longitudinal-mode thulium-doped fibre laser operating in the 2.0- μm band has a wide range of applications, and it is necessary to further study and optimize its performance. Single-longitudinal-mode fibre lasers have excellent and better power stability than the traditional semiconductor lasers, and their modulation amplitude does not change with the modulation frequency. However, there are very few reports on the 2.0- μm -band spatial optical network. The 2.0- μm -band wavelength division multiplexing system requires the single-longitudinal-mode and multi-wavelength thulium-doped fibre laser. In our study, we reported a three-wavelength-switchable single-longitudinal-mode thulium-doped fibre laser based on a Fabry-Perot fibre Bragg grating filter. Under the normal room temperature condition, this laser can obtain the single-longitudinal-mode, high stability, ultra-high optical signal-to-noise ratio, and high power output. Therefore, this study has an important application value in space optical communications.

Methods The experimental structure of the proposed laser is shown in Fig. 6. A 793-nm laser diode was used as the pump source, pumping a 2-m thulium-doped fibre. The circulator ensured the one-way operation of the optical path in the cavity; a three-channel narrow-band Fabry-Perot fibre Bragg grating filter and a fibre Bragg grating were fabricated using the phase-mask method. The fibre Bragg grating was placed on a translation stage and its reflection wavelength was changed using stress to make it overlap with each channel of the Fabry-Perot fibre Bragg grating. The optical signals passing through the filters can be selected and most of the longitudinal modes can be suppressed to vary the laser wavelength. The polarization controller balanced the gain and loss of the intracavity signal to stabilise the output with the highest optical signal-to-noise ratios. Two 50:50 couplers formed an 8-shaped sub-cavity, which effectively increased the longitudinal mode interval in the composite cavity, so that each channel of the Fabry-Perot fibre Bragg grating filter obtained single-longitudinal-mode lasing. The 10% port of the 90:10 coupler was used to output the laser, and the 90% port was connected to the main cavity. By reasonably adjusting the length of each resonant cavity, the single-longitudinal-mode output of the proposed laser was realized.

Results and Discussions The transmission spectrum of the self-made Fabry-Perot fibre Bragg grating filter had three narrow-band filtering channels with the centre wavelengths of 1941.48, 1941.57, and 1941.65 nm; the corresponding 3-dB bandwidths were 0.060, 0.054, and 0.066 nm, respectively. The 3-dB bandwidth of fibre Bragg grating was 0.11 nm and the reflectivity was $\sim 97\%$. The centre wavelength of the fibre Bragg grating was matched with the centre wavelength of the three transmission channels of Fabry-Perot fibre Bragg grating through a translation stage (Fig. 5). The designed 8-shaped sub-cavity expanded the longitudinal mode interval in the cavity to 0.3 nm, which was greater than the 3-dB bandwidth of each channel of the Fabry-Perot fibre Bragg grating filter, ensuring the single-longitudinal-mode lasing in each channel (Fig. 7). Switching between different laser wavelengths was achieved by changing the reflection wavelength of the fibre Bragg grating under the normal room temperature condition and the output lasers with three different wavelengths (Fig. 8). The wavelength fluctuations were less than the minimum resolution of optical spectrum analyser, which was 0.05 nm. Each lasing's power fluctuations were less than 0.39 dB, 0.61 dB, and 0.55 dB (Figs. 9 and 10). The experimental results indicated that the laser could work with a good stability in 50 min. Using a spectrum analyser to observe the frequency spectra of the output laser, it was seen that the laser worked at the single-longitudinal-mode operation stably (Fig. 11).

Conclusions In the present study, first, the Fabry-Perot fibre Bragg grating filter is analyzed theoretically. Based on the filter, a three-wavelength-switchable single-longitudinal-mode thulium-doped fibre laser is verified. Then, the narrow-band Fabry-Perot fibre Bragg grating and fibre Bragg grating are fabricated. The laser wavelength can be switched among three wavelengths by stretching the fibre Bragg grating in the cavity through regulating the stress adjustment frame. The laser works stably at the single-longitudinal-mode operation by adjusting the polarisation controller. An 8-shaped passive sub-cavity is employed to expand the longitudinal mode spacing. At 24 °C, the laser wavelengths were 1941.48, 1941.57, and 1941.65 nm and the corresponding optical signal-to-noise ratios were 61 dB, 61 dB, and 60 dB, respectively. The stability of lasing was measured in 50 min. The output power fluctuation of each lasing was less than 0.39, 0.61, and 0.55 dB, respectively. The wavelength fluctuations were less than 0.01 nm, which was less than the optical spectrum analyzer's minimum resolution of 0.05 nm. Therefore, the three-wavelength switchable thulium-doped fibre laser has stable single-longitudinal-mode output characteristics and can be applied to the fields of optical communication and optical fibre sensing in the 2.0- μm band.

Key words laser optics; thulium-doped fiber laser; single longitudinal mode; compound cavity; fiber Bragg grating; Fabry-Perot fiber Bragg grating filter

OCIS codes 140.3510; 140.3570; 140.3600